

Cite this paper: *Chin. J. Chem.* 2023, 41, 1727–1732. DOI: 10.1002/cjoc.202300039

Hierarchical Self-assembly of G-Quadruplexes Based Hydrogel Consisting of Guanine and Peptide Epitope[†]

Hongyue Zhang,^{a,b} Xuejiao Yang,^b Juan Liang,^b Kaihua Chen,^b and Huaimin Wang^{*a,b}

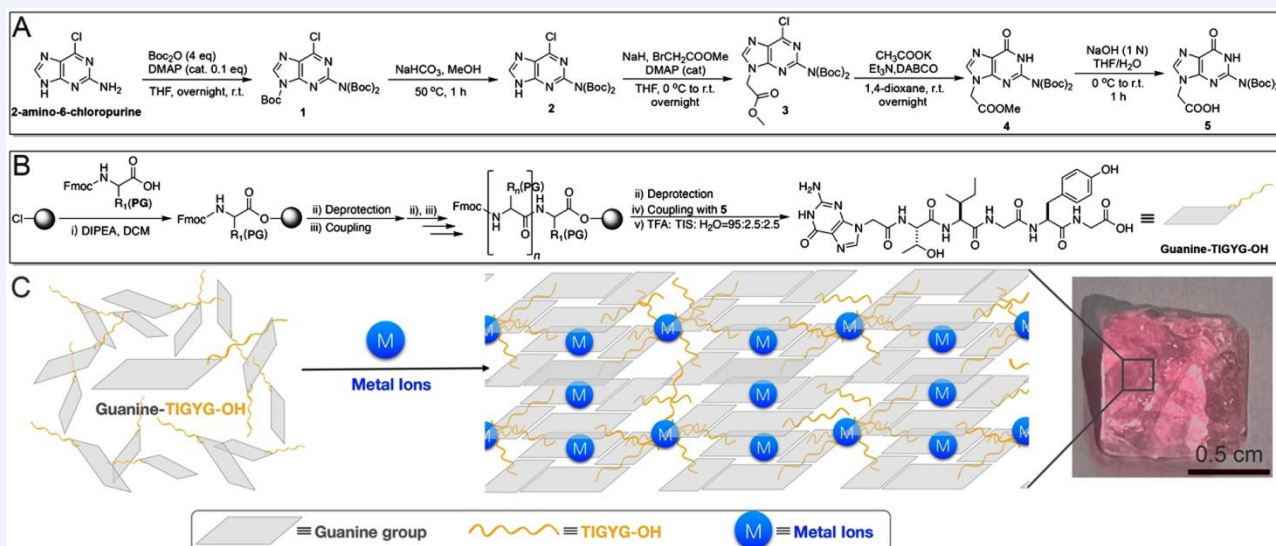
^a Department of Chemistry, Zhejiang University, Hangzhou, Zhejiang 310027, China

^b Key Laboratory of Precise Synthesis of Functional Molecules of Zhejiang Province, Department of Chemistry, School of Science, Westlake University; Institute of Natural Sciences, Westlake Institute for Advanced Study, No. 600 Dunyu Road, Hangzhou, Zhejiang 310024, China

Keywords

G-Quadruplexes | Peptides | Nucleobases | Self-assembly | Hydrogels | Cell culture

Comprehensive Summary



Guanosine-based hydrogels have attracted considerable attention because of their simplicity and easy preparation. However, the sugar moiety limits its further applications because of the necessity of sugar in the hydrogel formation. This work reports a G-quadruplexes-based hydrogel consisting of guanine and peptide epitope to form a supramolecular hydrogel in the presence of metal cations. Using the metal ion-responsive peptide epitope from the ion channel to replace sugar motif at N9 position of guanosine results in a novel nucleopeptide. The results show that the gelation time, the diameter of nanofibers, the anisotropic property, and the mechanical property of the hydrogel can be simply controlled using metal cations. The magnesium and calcium ions direct the alignment of nanofibers to form anisotropic nano-bundles. The mechanistic studies indicate the formation of G-quadruplexes in the hydrogel. Compared to the storage modulus of nucleopeptide without the metal cation, adding zinc ions results in an over three-order increase in mechanical properties. Cytotoxicity experiment indicates the good biocompatibility of our hydrogel. Moreover, we demonstrate that the guanine-capped peptide could release STING agonist in a controlled manner. This work illustrates a simple way to modulate the property of the nucleopeptide hydrogel to develop soft materials.

*E-mail: wanghuaimin@westlake.edu.cn

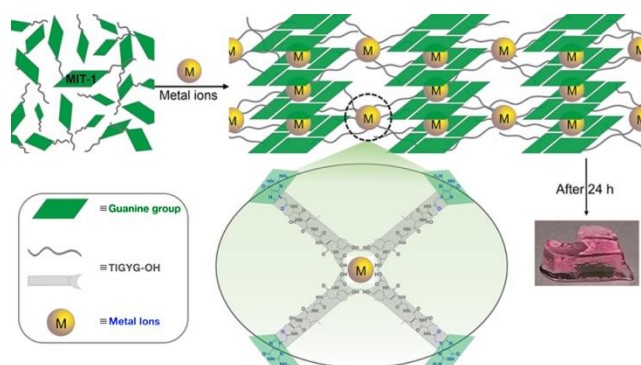
[†] Dedicated to the Special Issue of Hydrogels.

Background and Originality Content

Supramolecular hydrogel, consisting of water and a supramolecular gelator, has recently attracted increased attention. As an emerging material, supramolecular hydrogel has a variety of applications, including drug delivery,^[1-4] tissue engineering,^[5-6] analyte detection,^[7-8] wound healing,^[9-12] serving as an immunoadjuvant,^[13-15] and cancer inhibition.^[16-20] Guanosine, one of the natural small molecules, is an extensively explored small molecule for supramolecular hydrogel because of its simplicity and easy preparation. The reported works have discovered that the sugar moiety plays a vital role in determining the hydrogel formation of guanosine, which limits its further application in materials science and biomedicine. In recent years, nucleopeptides integrating nucleobase and amino acids have been introduced in material science to increase the stability and extend the gelator scope of hydrogels. Naturally, existing nucleopeptides are usually antibiotics and are used for treating microorganisms.^[21-22] Realization of internucleobase interaction can direct the self-assembly of nucleobase bola-amphiphiles, scientists have employed nucleopeptide as a building block for self-assembly. For example, Xu and co-workers found that simply conjugating a nucleobase to the self-assembled dipeptide or tripeptide could afford the hydrogel by adjusting pH or using an enzyme as a trigger.^[24-25] Suggs group also demonstrated that conjugating a nucleobase with tripeptides could form nanofibrous hydrogels through Watson-Crick base pairing and π - π stacking interactions.^[26-27] Several strategies have been introduced for generating supramolecular hydrogel of nucleopeptide, including pH adjustment, enzymatic reaction, and heating-cooling method. Each of these strategies could induce hydrogel formation efficiently. However, they also have several limitations to apply in physiological conditions. Moreover, the mechanical property of hydrogel formed by the above strategies could not be controlled easily.

Inspired by the detailed mechanical insight of the hydrogel formation of guanosine^[28] and the research interest in nucleopeptide, we hypothesized that introducing a metal ion-responsive peptide to replace the sugar moiety of guanosine could be a general strategy to construct G4-quartet hydrogel based on guanosine. Herein, this work reports a rationally designed nucleopeptide that could be driven by metal ions to generate biocompatible hydrogel with controlled mechanical properties. Our results (Scheme 1) indicate that **MIP-1** self-assembles to form soluble nanofibers in an aqueous solution. Adding metal ions induces the conformation changes of nanofibers, resulting in a hydrogel formation of **MIP-1** (Figure 1). Circular dichroism (CD) experiments and small-angle X-ray scattering (SAXS) analysis indicate that the optimized metal ions could induce the formation of G-quadruplex secondary structures in the hydrogels. Interestingly, the divalent metal ions (Mg^{2+} and Ca^{2+}) serve as a bridge to crosslink the nanofibers to form aligned nanobundles in the hydrogel, resulting in higher mechanical properties. Notably, the hydrogel induced by Zn^{2+}

Scheme 1 Schematic illustration of hydrogel formation of **MIP-1** in the presence of metal ions



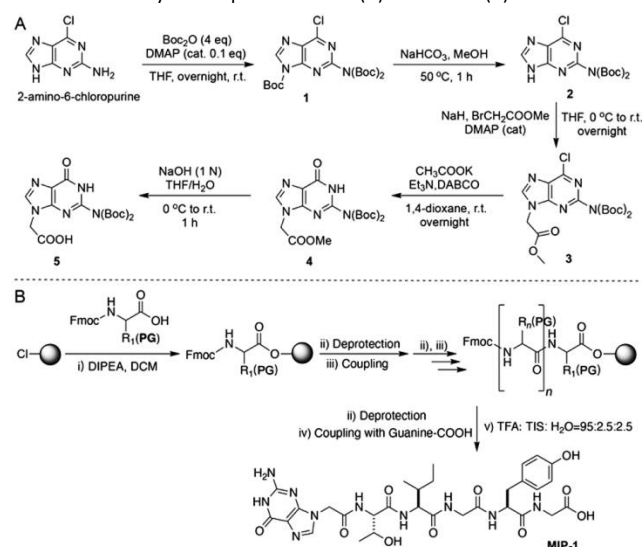
exhibits an over three order increase in the mechanical property compared to the original hydrogel. Cell experiments suggest the excellent biocompatibility of hydrogel. Moreover, we demonstrate that the guanine-capped peptide could release STING agonist cGAMP in a controlled manner, which could be useful for immunotherapy. This work provides a general strategy for constructing G4-quartet hydrogel with tunable mechanical properties and morphologies based on guanine.

Results and Discussion

Molecular design and synthesis

Unlike the previous reports, this work focuses on the ion-responsive peptide from the ion channel to replace the pentose of guanosine at the N⁹ position. Scheme 2 shows the representative structure of the designed molecule, which consists of guanine as a capping group and pentapeptide (TIGYG) from the potassium channel for interacting with ions.^[29-31] We also use different numbers of glycine as a linker to evaluate the influence of space between guanine and pentapeptide on the self-assembly property of resulted molecules.

Scheme 2 The synthetic processes of **5** (A) and **MIP-1** (B)



We first synthesized a guanosine derivative molecule **5** to obtain the designed molecules. Briefly, the exocyclic amine of 2-amino-6-chloropurine was protected by a Boc_2O group resulting in **1**, and the amine of the purine ring was alkylated with methyl bromoacetate to yield **2**. We obtained **5** by displacing the chlorine at the C-6 position with oxo-group in the parent nucleus and the following hydrolysis process by saturated sodium bicarbonate ($NaHCO_3$). After the purification of **5**, we used Fmoc solid-phase peptide synthesis to obtain the designed molecules. After high-performance liquid chromatography (HPLC) purification, NMR spectra and LC-MS analysis confirm the structures and purities of the designed precursors (Table S1, Figures S1–16).

Gelation properties and the morphologies of hydrogel

We first evaluated the gelation properties of guanine at a higher concentration (4 mmol/L). The results showed that the guanine could not form a hydrogel regardless of the presence of metal ions in Tris buffer (Figure S32), consistent with the previous reports.^[28] In contrast, **MIP-1** could form a stable hydrogel in the presence of KCl with the critical gelation concentration (CGC) of 3.75 mmol/L (Figures S17 and 18). We next evaluated the gelation properties of **MIP-1** in the presence of different metal ions (Figure 1A and Figure S19). Specifically, **MIP-1** forms an opaque hydrogel upon adding Mg^{2+} or Ca^{2+} , and we could observe the formation of

transparent hydrogels in the presence of other metal ions. Moreover, we were curious about the influence of pH on the gelation properties of **MIP-1** in the presence of metal ions. At pH 5.0, all metal ions could trigger the **MIP-1** to form hydrogels (Figure S22). At pH 9.0, addition of the alkali metal ions could not induce **MIP-1** to form hydrogel. While Mg^{2+} , Ca^{2+} and Al^{3+} could trigger **MIP-1** to form opaque hydrogels, and Zn^{2+} (or Cu^{2+}) could induce **MIP-1** to form opaque solutions (Figure S23). These results suggested that pH had a significantly influence on the gelation properties of nucleopeptides. Replacing the guanine capping group with acetyl-group to result in **Ac-MIP** could not form a hydrogel (Figure S20), indicating the vital role of guanine in constructing G4-quartet hydrogels. We used glycine as a linker between guanine and peptide epitope to demonstrate the spacer's role in the hydrogel formation. The results indicated that the shorter of the linker between guanine and the peptide epitope, the easier to form a hydrogel of nucleopeptide (Figure S21).

Cryo-electron microscope (Cyro-EM, Figure 1) indicates the diameter of nanofibers formed by **MIP-1** is 6 ± 1 nm. Adding alkali metal ions (Li^+ , Na^+ , K^+) hardly changes the diameter of the nanofibers but could induce **MIP-1** to form a hydrogel. The alkaline-earth metal ions (Mg^{2+} and Ca^{2+}) could trigger **MIP-1** to form nano-bundles through the interactions between nanofibers. The morphologies of hydrogel formed by **MIP-1** in the presence of Zn^{2+} are similar to monovalent cation ions, while the hydrogels induced by Cu^{2+} or Al^{3+} exhibited short nanofibers with a diameter of around 6 nm. These results suggested that using metal ions to crosslink the pre-existing nanofibers is an efficient method to form a hydrogel of nucleopeptide.

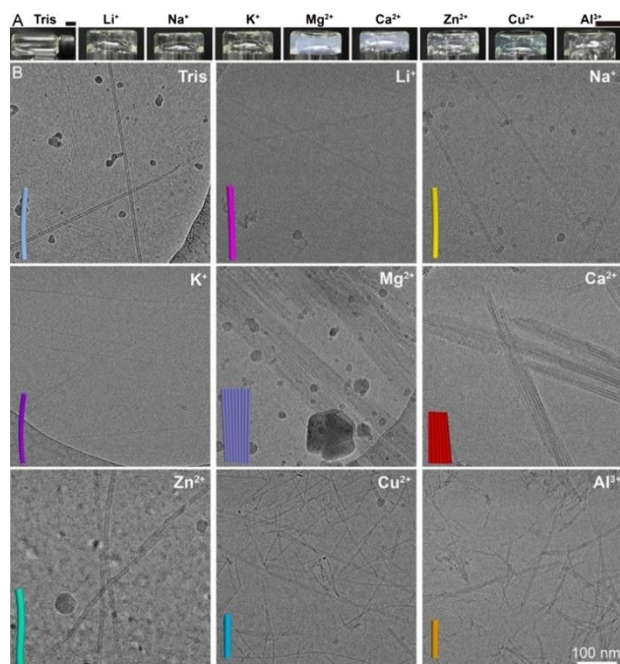


Figure 1 (A) Optical images and (B) Cryo-EM images of **MIP-1** (4 mmol/L) without or with the addition of different metal ions (40 mmol/L). Scale bar of A and B are 0.5 cm and 100 nm, respectively.

Characterization of the hydrogel

To investigate the turbidity of hydrogels formed by **MIP-1** upon the treatment of different metal ions, we first measured the UV spectra of free peptides in tris buffer. All peptides exhibited no absorbance at the wavelength of 405 nm, indicating that the absorption of peptides could not affect the results and displayed the real value of turbidity properties (Figure S24). The turbidity experiment (Figure 2A) indicated that the hydrogel induced by Mg^{2+} exhibited the highest absorbance value, followed by the hydrogels formed by Ca^{2+} and Cu^{2+} , consistent with the observation by opti-

cal experiments (Figure 1A). The turbidity of the hydrogels formed by monovalent cation ions (Li^+ , Na^+ , K^+) was similar to the solution of **MIP-1**, while the hydrogels formed by Al^{3+} and Zn^{2+} exhibited a higher value. The turbidity of Li^+ , Na^+ , K^+ hydrogels were the lowest and could form transparent hydrogels (Figure 1A). We used circular dichroism (CD) to investigate the secondary structures of hydrogels. G-quadruplex has three typical types of tertiary structures (hybrid, parallel and anti-parallel) with distinctive CD signals. As shown in Figure 2B, the hydrogels formed by Mg^{2+} , Ca^{2+} , Zn^{2+} , Cu^{2+} and Al^{3+} exhibited the anti-parallel G-quadruplex structure, bearing two positive peaks at ~ 240 nm and ~ 295 nm and a negative peak at ~ 260 nm, respectively. The hydrogels formed by the monovalent cation ions (Li^+ , Na^+ , K^+) exhibited similar trend, but the signal was weak with blue shift (Figure S25). These results showed that the tertiary structures were formed in all metal ions-induced hydrogels and multivalent metal ions could form tighter structures.

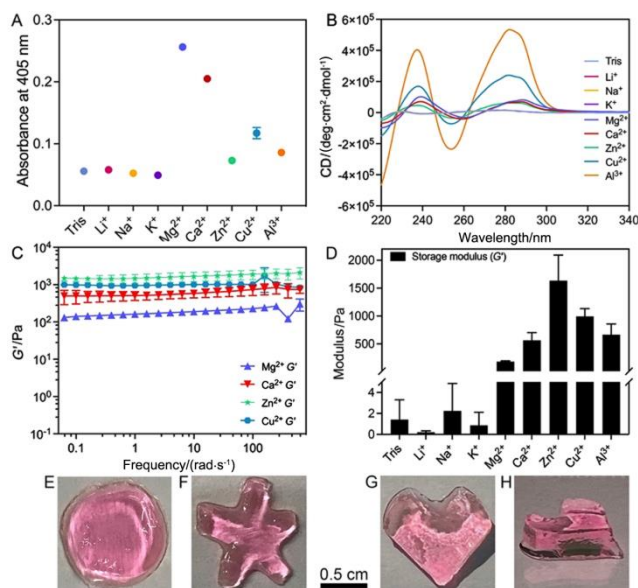


Figure 2 (A) Turbidity assays of the **MIP-1** hydrogels upon the treatment of metal ions for 24 h. (B) CD spectra of **MIP-1** without or with adding metal ions. (C) Dynamic frequency sweep of **MIP-1** (4 mmol/L) in the presence of 40 mmol/L Mg^{2+} , Ca^{2+} , Zn^{2+} and Cu^{2+} with a strain of 0.5%. (D) The summary plot of rheological profiles of the hydrogel formed by **MIP-1** (4 mmol/L) treating with different metal ions (40 mmol/L) after 24 h. (E–H) The optical images of hydrogels formed by **MIP-1** (4 mmol/L) and Zn^{2+} (40 mmol/L). 5 $\mu\text{mol/L}$ rhodamine 6G (Rho 6G) was used to indicate the shape of the hydrogel.

We next used the rheometer to examine the viscoelastic properties of the hydrogels. After determining the proper condition for the dynamic frequency sweep of the hydrogel by the dynamic strain sweep (Figure S26), we characterized and summarized the storage modulus (G') of the hydrogels (Figure 2D). The results indicate (Figure 2C and Figure S27) that G' is larger than the loss modulus (G'') of the hydrogels formed by divalent metal ions (Mg^{2+} , Ca^{2+} , Zn^{2+} , Cu^{2+}), and the G' slightly changes with the increase of frequency (0.01 to 100 Hz), suggesting these hydrogels are tolerant to external shear force. The mechanical properties of the hydrogels (Figure 2D) follow the order of $\text{Zn}^{2+} > \text{Cu}^{2+} > \text{Al}^{3+} > \text{Ca}^{2+} > \text{Mg}^{2+} > \text{Na}^+ > \text{K}^+ > \text{Li}^+$, indicating that the divalent and trivalent metal ions could form hydrogels with stronger mechanical properties than monovalent metal ions. The reason could be due to that the diameter of multivalent ions is more suitable for the size of the G4 hole than that of alkali metal ions. The results indicate that **MIP-1** could form the viscous solution, consistent with the result of TEM. These results also implied that the pre-formed nanofibers are insufficient for hydrogel formation. Adding metal

ions could crosslink these nanofibers to induce hydrogel formation. To evaluate the plastic property of the hydrogels, we also made mesoscale hydrogel into different shapes (Figures 2E to 2H). The results indicate that the hydrogel has the suitable plasticity to be tailored to various shapes.

Energy dispersive spectroscopy (EDS) revealed the existence of metal ions on the nanofibers (Figure S28A), suggesting the interaction of nanofibers with metal ions. The small-angle X-ray scattering (SAXS) patterns (Figure S28B) show that the hydrogel displayed the 5.04 Å and 7–8 Å diffractions, attributing to the periodic interlamellar between G4-quartet. The refractive index of crystals and highly-aligned materials changed with the polarization of the light, which is defined as the birefringence properties.^[32] As shown in Figure 3, the degree of polarization and the polarization azimuth angle in the hydrogel were displayed by the orientation pseudo image. The hydrogels formed by adding Li⁺, Na⁺, K⁺, Mg²⁺, Ca²⁺, and Zn²⁺ contain highly birefringent domains, indicating the anisotropic properties of nanofibers. Whereas the hydrogels formed by **MIP-1** with Cu²⁺, Al³⁺ exhibit a low birefringence, indicating the isotropy property of these nanofibers.

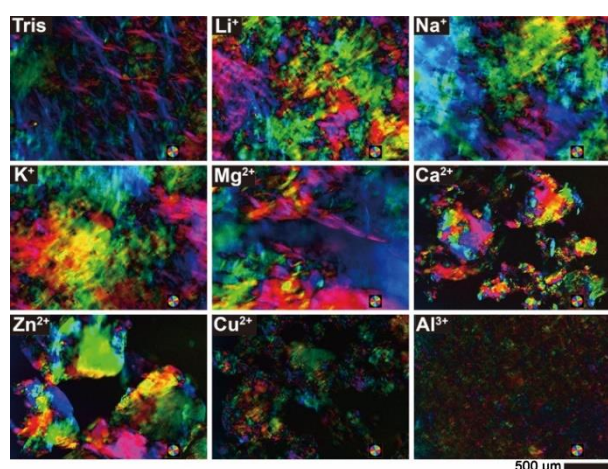


Figure 3 Polarizing optical microscope images of **MIP-1** (4 mmol/L) upon the treatment of different metal ions (40 mmol/L) for 24 h.

Biocompatibility and the application of the hydrogel

The biocompatibility of the hydrogel is a key factor for its applications in biomedical areas. The live-dead experiment (Figures 4A and B) indicates that HeLa cells on the K⁺ hydrogel exhibited green fluorescence, indicating that all the cells are alive. We also used tubulin tracker (Figures S29–30) to detect the changes in cytoskeletons of HeLa cells on the hydrogel. The results suggest the cells spread well on the hydrogel without detectable cytotoxicity (Figure S31). Since the hydrogels in our system contain guanine, we wonder if the hydrogel could control the release of cGAMP (Cyclic GMP-AMP), a STING activator bearing similar structure to guanine.^[33] The results showed that the cGAMP encapsulated in the hydrogels could be gradually released with the increase of time (Figure 4C and Figure S33). Specifically, the hydrogels released cGAMP at a fast rate at first 10 h, and then at a relatively lower rate per hour in the following hours. After 48 h, 92% of cGAMP was released in K⁺ hydrogel, while 88% of cGAMP could be released from the Zn²⁺ hydrogel. The degradation experiments revealed that the guanine modification could delay the degradation of the system in the presence of proteinase K (Figure 4D), suggesting the stability of the hydrogel.

Conclusions

In summary, this work developed a G4-quartet hydrogel without sugar based on guanine and peptide epitope. We demonstrated the metal ions severed as a bridge to crosslink the existing

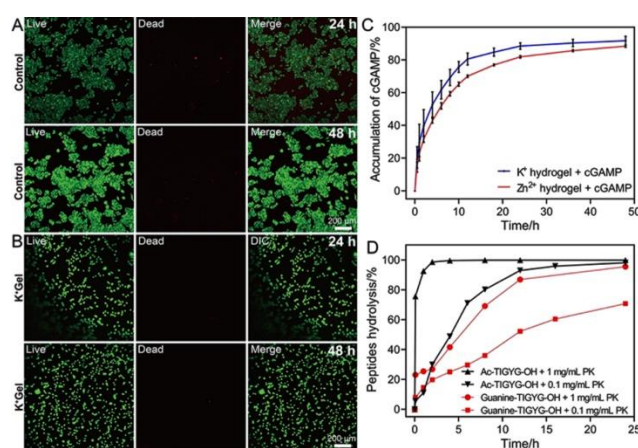


Figure 4 Live-dead assays of HeLa cells incubated on the (A) tissue-culture polystyrene surface, and (B) the hydrogel for 24 h and 48 h, respectively. (C) Accumulative release profile of cGAMP from different hydrogels. (D) Degradation of **Ac-MIP** (4 mmol/L) and **MIP-1** (4 mmol/L) in the presence of proteinase K for 24 h.

nanofibers to tune the phase transition of **MIP-1** from the solution to a hydrogel. The mechanical properties of the hydrogel could be easily tuned by adding different metal ions. Specifically, Zn²⁺ hydrogel had the highest storage modulus and could be cut into different shapes as well. Our results also indicated that the anisotropy and isotropy of the hydrogel could be obtained by using different metal ions, Mg²⁺, Ca²⁺ and Zn²⁺ induced **MIP-1** to form anisotropic hydrogels with strong birefringent intensity, while Cu²⁺ and Al³⁺ induced G4-quartet hydrogels to form isotropic hydrogels. The resulting hydrogels exhibited excellent biocompatibility and are suitable for drug delivery (K⁺ and Zn²⁺ triggered G4-quartet hydrogels). This work provides a platform for designing soft materials of nucleopeptides which could be used in drug delivery and tissue engineering.

Experimental

Materials

Starting materials, dry solvents and reagents were purchased from commercial suppliers and used directly without further purification. 2-Chlorotriethyl chloride resin was from Tianjin Nankai HECHENG S&T Co., Ltd. Fluorenylmethyloxycarbonyl (Fmoc) protected amino acids and 2-(1*H*-benzotriazol-1-yl)-1,1,3,3-tetramethyluronium hexafluorophosphate (HBTU) were brought from GL Biochem (Shanghai, China). Rhodamine 6G, metal chloride salts were purchased from Aladdin Industrial Co., Ltd. (Shanghai, China). Uranyl acetate was purchased from Aladdin Industrial Co., Ltd. (Shanghai, China). Cell counting kit 8 (CCK-8) was brought from Abcom. Minimal essential medium (MEM), fetal bovine serum (FBS), 0.25% trypsin-EDTA, live cell imaging solution, Tubulin Tracker™ Green and live/dead assay were purchased from Gibco (Thermo fisher scientific, US).

Preparation of peptides

All the peptides were obtained by standard solid phase peptide synthesis (SPPS) using 2-chlorotriethyl chloride resin (Scheme S1).

Turbidity assay

90 μL of **MIP-1** (4.44 mmol/L) solution and 10 μL of different metal ions (400 mmol/L) in tris buffer (pH 7.4) were mixed together to reach the final concentration of 4 mmol/L (nucleopeptide) and 40 mmol/L (metal ion), respectively. The mixture was put into a 96-well plate at room temperature. The UV absorbance was determined after 24 h at the wavelength of 405 nm.

Circular dichroism (CD)

CD (Applied Photophysics Ltd, UK) of different samples was measured from 220 nm to 340 nm with 0.1 nm interval for three times. The ellipticity (mdeg) signal was obtained and converted to mean molar ellipticity ($\text{deg}\cdot\text{cm}^2\cdot\text{dmol}^{-1}$) by the following equation:

$$[\theta] = \theta \cdot 1000 / c \cdot l$$

where θ is the recorded ellipticity in mdeg, c is the concentration of the sample in mmol/L, and l is the light path length of quartz cuvette in 0.1 mmol/L. Data processing was performed via Pro-Data Viewer software.

Rheology

Rheological experiment was recorded by using a rheometer ARES-G2 (TA-Waters, USA) via a 25 mm standard parallel-plate geometry under 0.5 mm gap at 25 °C.

EDS mapping

The SEM-ready samples were obtained on the silicon slice. The distribution of metal ions was detected using an Ultim EX-TREME (Regulus 8230 electron microscope) and operating at 5 kV accelerating voltage.

Small angle X-ray scattering (SAXS)

SAXS measurements were performed *in situ* on a XENOCs instrument using a CuK α radiation (1.5418 Å) and a PILATUS 100 K detector. SAXS profiles were measured at a sample-to-detector distance of 570 mm.

Polarized light microscopy (POM) images of hydrogels

After the formation of the hydrogels for 24 h, the hydrogels were placed on a microscope glass slide and recorded by Oosight macroscopy.

cGAMP release profiles from the hydrogels

During the hydrogel formation, we added 300 $\mu\text{mol/L}$ cGAMP in the solution. After 24 h, we added 300 μL tris buffer on the surface of hydrogel. At designated time points (0.5 h, 1 h, 2 h, 4 h, 6 h, 8 h, 10 h, 12 h, 18 h, 24 h, 36 h and 48 h, respectively), we carefully took out 150 μL sample solution and added back 150 μL tris buffer solution. The sample solutions were filtered by 0.22 μm filter and determined by analytical HPLC. The experiments were repeated for six times.

Live-dead assay

After the formation of the hydrogel onto the 96-well plate, we used the MEM cell culture medium to exchange the solvents (tris buffer) for three times, and put the HeLa cells (1×10^4) on the surface of hydrogels slowly. After 24 h or 48 h, we added the live-dead staining solution into the cells for another 1 h and detected by Zeiss LSM800 CLSM (Zeiss, Germany).

Tubulin staining experiment

After the formation of the hydrogel onto a 3.5 mm confocal dish, we used the MEM cell culture medium to exchange the solvents (tris buffer) for three times and put the HeLa cells (1×10^5) onto the surface of hydrogels slowly. After 24 h and 48 h, we added the tubulin staining solution into the cells for another 1 h and detected them by Zeiss LSM800 CLSM (Zeiss, Germany).

Supporting Information

The supporting information for this article is available on the WWW under <https://doi.org/10.1002/cjoc.202300039>.

Acknowledgement

This work is supported by the National Natural Science Founda-

tion of China (82022038). We thank the Instrumentation and Service Center for Molecular Sciences, Physical Sciences, and Biomedical Research Core Facilities at Westlake University.

References

- [1] Gao, Y.; Kuang, Y.; Guo, Z.-F.; Guo, Z.; Krauss, I. J.; Xu, B. Enzyme-Instructed Molecular Self-assembly Confers Nanofibers and a Supramolecular Hydrogel of Taxol Derivative. *J. Am. Chem. Soc.* **2009**, *131*, 13576–13577.
- [2] Du, X.; Zhou, J.; Shi, J.; Xu, B. Supramolecular Hydrogelators and Hydrogels: From Soft Matter to Molecular Biomaterials. *Chem. Rev.* **2015**, *115*, 13165–13307.
- [3] Li, J.; Mooney, D. J. Designing hydrogels for controlled drug delivery. *Nat. Rev. Mater.* **2016**, *1*, 16071.
- [4] Shi, Q.; Liu, H.; Tang, D.; Li, Y.; Li, X.; Xu, F. Bioactuators based on stimulus-responsive hydrogels and their emerging biomedical applications. *NPG Asia Mater.* **2019**, *11*, 64.
- [5] Ikeda, M.; Tanida, T.; Yoshii, T.; Kurotani, K.; Onogi, S.; Urayama, K.; Hamachi, I. Installing logic-gate responses to a variety of biological substances in supramolecular hydrogel–enzyme hybrids. *Nat. Chem.* **2014**, *6*, 511–518.
- [6] Zhao, Y.; Song, S.; Ren, X.; Zhang, J.; Lin, Q.; Zhao, Y. Supramolecular Adhesive Hydrogels for Tissue Engineering Applications. *Chem. Rev.* **2022**, *122*, 5604–5640.
- [7] Sun, B.; Tao, K.; Jia, Y.; Yan, X.; Zou, Q.; Gazit, E.; Li, J. Photoactive properties of supramolecular assembled short peptides. *Chem. Soc. Rev.* **2019**, *48*, 4387–4400.
- [8] Kim, J. H.; Lim, S. Y.; Nam, D. H.; Ryu, J.; Ku, S. H.; Park, C. B. Self-assembled, photoluminescent peptide hydrogel as a versatile platform for enzyme-based optical biosensors. *Biosens. Bioelectron.* **2011**, *26*, 1860–1865.
- [9] Xiao, M.; Gao, L.; Chandrasekaran, A. R.; Zhao, J.; Tang, Q.; Qu, Z.; Wang, F.; Li, L.; Yang, Y.; Zhang, X.; Wan, Y.; Pei, H. Bio-functional G-molecular hydrogels for accelerated wound healing. *Mater. Sci. Eng. C* **2019**, *105*, 110067.
- [10] Zhou, Y.; Qiu, P.; Yao, D.; Song, Y.; Zhu, Y.; Pan, H.; Wu, J.; Zhang, J. A crosslinked colloidal network of peptide/nucleic base amphiphiles for targeted cancer cell encapsulation. *Chem. Sci.* **2021**, *12*, 10063–10069.
- [11] Sonamuthu, J.; Cai, Y.; Liu, H.; Kasim, M. S. M.; Vasanthakumar, V. R.; Pandi, B.; Wang, H.; Yao, J. MMP-9 responsive dipeptide-templated natural protein hydrogel-based wound dressings for accelerated healing action of infected diabetic wound. *Int. J. Biol. Macromol.* **2020**, *153*, 1058–1069.
- [12] Wu, J.; Li, P.; Dong, C.; Jiang, H.; Xue, B.; Gao, X.; Qin, M.; Wang, W.; Chen, B.; Cao, Y. Rationally designed synthetic protein hydrogels with predictable mechanical properties. *Nat. Commun.* **2018**, *9*, 1–11.
- [13] Wang, Y.; Jiang, Z.; Xu, W.; Yang, Y.; Zhuang, X.; Ding, J.; Chen, X. Chiral Polypeptide Thermogels Induce Controlled Inflammatory Response as Potential Immunoadjuvants. *ACS Appl. Mater. Interfaces* **2019**, *11*, 8725–8730.
- [14] Luo, Z.; Wu, Q.; Yang, C.; Wang, H.; He, T.; Wang, Y.; Wang, Z.; Chen, H.; Li, X.; Gong, C.; Yang, Z. A Powerful CD8+ T-Cell Stimulating D-Tetra-Peptide Hydrogel as a Very Promising Vaccine Adjuvant. *Adv. Mater.* **2017**, *29*, 1601776.
- [15] Wang, H.; Luo, Z.; Wang, Y.; He, T.; Yang, C.; Ren, C.; Ma, L.; Gong, C.; Li, X.; Yang, Z. Enzyme-Catalyzed Formation of Supramolecular Hydrogels as Promising Vaccine Adjuvants. *Adv. Funct. Mater.* **2016**, *26*, 1822–1829.
- [16] Wang, F.; Su, H.; Xu, D.; Dai, W.; Zhang, W.; Wang, Z.; Anderson, C. F.; Zheng, M.; Oh, R.; Wan, F.; Cui, H. Tumour sensitization via the extended intratumoural release of a STING agonist and camptothecin from a self-assembled hydrogel. *Nat. Biomed. Eng.* **2020**, *4*, 1090–1101.
- [17] Gao, G.; Jiang, Y.-W.; Zhan, W.; Liu, X.; Tang, R.; Sun, X.; Deng, Y.; Xu, L.; Liang, G. Trident molecule with nanobrush–nanoparticle–nanofiber transition property spatially suppresses tumor metastasis.

- J. Am. Chem. Soc.* **2022**, *144*, 11897–11910.
- [18] Feng, Z.; Wang, H.; Chen, X.; Xu, B. Self-assembling ability determines the activity of enzyme-instructed self-assembly for inhibiting cancer cells. *J. Am. Chem. Soc.* **2017**, *139*, 15377–15384.
- [19] Cai, Y.; Shen, H.; Zhan, J.; Lin, M.; Dai, L.; Ren, C.; Shi, Y.; Liu, J.; Gao, J.; Yang, Z. Supramolecular “Trojan Horse” for nuclear delivery of dual anticancer drugs. *J. Am. Chem. Soc.* **2017**, *139*, 2876–2879.
- [20] Pires, R. A.; Abul-Haija, Y. M.; Costa, D. S.; Novoa-Carballal, R.; Reis, R. L.; Ulijn, R. V.; Pashkuleva, I. Controlling cancer cell fate using localized biocatalytic self-assembly of an aromatic carbohydrate amphiphile. *J. Am. Chem. Soc.* **2015**, *137*, 576–579.
- [21] Roviello, G. N.; Benedetti, E.; Pedone, C.; Bucci, E. M. Nucleobase-containing peptides: an overview of their characteristic features and applications. *Amino Acids* **2010**, *39*, 45–57.
- [22] Hector, R. F.; Zimmer, B. L.; Pappagianis, D. Evaluation of nikkomycins X and Z in murine models of coccidioidomycosis, histoplasmosis, and blastomycosis. *Antimicrob. Agents Chemother.* **1990**, *34*, 587–93.
- [23] Shimizu, T.; Iwaura, R.; Masuda, M.; Hanada, T.; Yase, K. Internucleobase-interaction-directed self-assembly of nanofibers from homo- and heteroditopic 1,ω-nucleobase bolaamphiphiles. *J. Am. Chem. Soc.* **2001**, *123*, 5947–5955.
- [24] Li, X.; Kuang, Y.; Lin, H.-C.; Gao, Y.; Shi, J.; Xu, B. Supramolecular Nanofibers and Hydrogels of Nucleopeptides. *Angew. Chem. Int. Ed.* **2011**, *50*, 9365–9369.
- [25] Li, X.; Yi, K.; Shi, J.; Gao, Y.; Lin, H.-C.; Xu, B. Multifunctional, Biocompatible Supramolecular Hydrogelators Consist Only of Nucleobase, Amino Acid, and Glycoside. *J. Am. Chem. Soc.* **2011**, *133*, 17513–17518.
- [26] Baek, K.; Noblett, A. D.; Ren, P.; Suggs, L. J. Design and characterization of nucleopeptides for hydrogel self-assembly. *ACS Appl. Bio Mater.* **2019**, *2*, 2812–2821.
- [27] Noblett, A. D.; Baek, K.; Suggs, L. J. Controlling Nucleopeptide Hydrogel Self-Assembly and Formation for Cell-Culture Scaffold Applications. *ACS Biomater. Sci. Eng.* **2021**, *7*, 2605–2614.
- [28] Guschlbauer, W.; Chantot, J.-F.; Thiele, D. Four-stranded nucleic acid structures 25 years later: from guanosine gels to telomer DNA. *J. Biomol. Struct. Dyn.* **1990**, *8*, 491–511.
- [29] Kuang, Y.; Gao, Y.; Shi, J.; Lin, H.-C.; Xu, B. Supramolecular hydrogels based on the epitope of potassium ion channels. *Chem. Commun.* **2011**, *47*, 8772–8774.
- [30] D'Avanzo, N.; Pekhletski, R.; Backx, P. H. P-loop residues critical for selectivity in K channels fail to confer selectivity to rabbit HCN4 channels. *PLoS One* **2009**, *4*, e7712.
- [31] Seebohm, G.; Westenskow, P.; Lang, F.; Sanguinetti, M. C. Mutation of colocalized residues of the pore helix and transmembrane segments S5 and S6 disrupt deactivation and modify inactivation of KCNQ1 K⁺ channels. *J. Physiol.* **2005**, *563*, 359–368.
- [32] Wu, B.; Zhao, S.; Yang, X.; Zhou, L.; Ma, Y.; Zhang, H.; Li, W.; Wang, H. Biomimetic Heterodimerization of Tetrapeptides to Generate Liquid Crystalline Hydrogel in A Two-Component System. *ACS Nano* **2022**, *16*, 4126–4138.
- [33] Wang, F.; Su, H.; Xu, D.; Dai, W.; Zhang, W.; Wang, Z.; Anderson, C. F.; Zheng, M.; Oh, R.; Wan, F. Tumour sensitization via the extended intratumoural release of a STING agonist and camptothecin from a self-assembled hydrogel. *Nat. Biomed. Eng.* **2020**, *4*, 1090–1101.

Manuscript received: January 24, 2023

Manuscript revised: March 13, 2023

Manuscript accepted: March 14, 2023

Accepted manuscript online: March 17, 2023

Version of record online: April 21, 2023

The Authors



Left to Right: Hongyue Zhang, Xuejiao Yang, Juan Liang, Kaihua Chen, and Huaimin Wang